Optical Engineering

OpticalEngineering.SPIEDigitalLibrary.org

Metallic and dielectric metasurfaces in photoconductive terahertz devices: a review

Alexander E. Yachmenev
Denis V. Lavrukhin
Igor A. Glinskiy
Nikolay V. Zenchenko
Yurii G. Goncharov
Igor E. Spektor
Rustam A. Khabibullin
Taiichi Otsuji
Dmitry S. Ponomarev

SPIE.

Alexander E. Yachmenev, Denis V. Lavrukhin, Igor A. Glinskiy, Nikolay V. Zenchenko, Yurii G. Goncharov, Igor E. Spektor, Rustam A. Khabibullin, Taiichi Otsuji, Dmitry S. Ponomarev, "Metallic and dielectric metasurfaces in photoconductive terahertz devices: a review," *Opt. Eng.* **59**(6), 061608 (2019), doi: 10.1117/1.OE.59.6.061608.

REVIEW

Metallic and dielectric metasurfaces in photoconductive terahertz devices: a review

Alexander E. Yachmenev,[a,b] Denis V. Lavrukhin,[a,b] Igor A. Glinskiy,[a,c] Nikolay V. Zenchenko,[a,c] Yurii G. Goncharov,[b] Igor E. Spektor,[b] Rustam A. Khabibullin,[a,c,d] Taiichi Otsuji,[e] and Dmitry S. Ponomarev[a,b,d,*]

[a]Russian Academy of Sciences, Institute of Ultra High Frequency Semiconductor Electronics, Moscow, Russia

[b]Russian Academy of Sciences, Prokhorov General Physics Institute, Moscow, Russia

[c]Bauman Moscow State Technical University, Moscow, Russia

[d]Moscow Institute of Physics and Technology, Dolgoprudny, Russia

[e]Tohoku University, Research Institute for Electrical Communication, Sendai, Japan

Abstract. This review highlights recent and novel trends focused on metallic (plasmonic) and dielectric metasurfaces in photoconductive terahertz (THz) devices. We demonstrate the great potential of its applications in the field of THz science and technology, nevertheless indicating some limitations and technological issues. From the state-of-the-art, the metasurfaces are, by far, able to force out previous approaches like photonic crystals and are capable of significantly increasing the performance of contemporary photoconductive devices operating at THz frequencies. © *2019 Society of Photo-Optical Instrumentation Engineers (SPIE)* [DOI: 10.1117/1.OE.59.6.061608]

Keywords: terahertz (THz) radiation; photoconductive antenna; THz emitters and detectors; plasmonic metasurface; dielectric metasurface; THz science and technology.

Paper 191515SSV received Oct. 30, 2019; accepted for publication Nov. 22, 2019; published online Dec. 10, 2019.

1 Introduction

To date, the terahertz (THz) frequency range has found wide applications in many fields ranging from condensed matter physics[1–4] and material science[5,6] to gas sensing[7–9] and pharmaceutical industry[10] as well as various security[11–16] and biomedical[17–22] applications. All of these require high-sensitive and broadband THz instruments, in particular, efficient operation in real time and at room temperature.[23,24]

Among the variety of contemporary THz emitters and detectors, photoconductive antennas (PCAs) have become the prevalent ones and currently are widely used as key elements in pulse and continuous-wave (CW) THz spectroscopic and imaging systems due to their reliability, cost effectiveness, relative ease of fabrication, and flexibility in design. Being used with femtosecond lasers, the PCAs exhibit a broad spectrum of up to 4.5 THz with a high dynamic range even exceeding 100 dB at room temperature. Nevertheless, PCAs' efficiency is limited by the amount of the energy of an absorbed optical radiation, relatively low mobility of photocarriers in photoconductive substrates,[25–27] screening effects,[28,29] and a semiconductor breakdown threshold voltage.[30,31] The increase in the PCA performance is predominantly associated with an efficient optical light confinement in the antenna's gap that can be reached due to metasurface implementation. The latter allows the manipulation of phase, amplitude, and polarization of an incident radiation with high spatial resolution. To date, two kinds of metasurfaces based on various principles are commonly used in PCA technology: metallic and dielectric metasurfaces.

The earlier works on metallic metasurfaces with different shapes and orientations have demonstrated resonant scattering of light by oscillating free electrons at the surface, which occurs due to a resonant electronic–electromagnetic oscillation providing high electromagnetic field enhancement.[32] In general, metallic (or plasmonic) metasurfaces exhibit better device

*Address all correspondence to Dmitry S. Ponomarev, E-mail: ponomarev_dmitr@mail.ru

performance yet suffer from high dissipation (ohmic) losses, making the on-chip power scaling with number of devices extremely inefficient.[33]

This drawback can be circumvented using dielectric metasurfaces, which consist of interfaces patterned with a distribution of high-index dielectric light scattering particles of size comparable[33] or shorter[34–37] than the wavelength of light. A fundamental difference from the traditional field enhancement seen in plasmonic metasurfaces is the achievement of not only electric field hotspots but also nanoscale magnetic hotspots exploiting magnetic Mie resonances and light enhancement by particle surface nanostructures.[38] Another unique aspect of dielectric metasurfaces lies in the great variety of possibilities for engineering the anisotropy of the media providing a light confinement without using metallic components. In general, dielectric metasurfaces can alter the wavefront of incident light for applications such as flat lenses,[39,40] polarizers, and beam shaping.[41,42] Their dielectric nature ensures higher transmission and diffraction efficiencies compared with plasmonic metasurfaces.

In addition, it should be noted that sufficiently small spherical dielectric nanoparticles provide pronounced resonances associated with the excitation of both magnetic and electric dipolar modes compared with plasmonic structures. Moreover, magnetic dipole modes also occur in dielectric particles with nonspherical geometries. In rectangular resonators, for example, the resonant wavelength can easily be tuned by changing either the geometry or the size of the scatterer.[43]

In this review, we briefly summarize some of the recent approaches aimed at the enhancement of optical-to-THz conversion efficiency in PCAs by implementation of various metallic and dielectric metasurfaces in the antenna's photoconductive gap. The paper is organized as follows. In Sec. 2, we consider the PCAs with metallic nanostructures featuring different geometries for generation and detection of THz waves. We concentrate on various approaches that utilize two-dimensional and three-dimensional plasmonic gratings and are aimed at the field enhancement. In Sec. 3, we focus on the dielectric nanostructures and highlight some recent PCA designs with new antireflection and protection coating layers as well as all-dielectric metasurfaces.

2 Metallic Metasurfaces

The implementation of metallic (plasmonic) structures into a PCA's gap leads to an increase of a photocarrier generation in a photoconductive layer, which results in an increased THz emission due to local field enhancement. This enhancement occurs due to surface plasmon waves[44] so that the field enhancement near the electrodes becomes much greater than the electric field of the incident wave.[45,46]

The idea to use plasmonic metasurface to manipulate the optical wave and to increase the efficiency of PCA started with the discovery of extraordinary optical transmission through subwavelength nanostructured arrays.[47] The authors found the unusual optical properties that are related to the coupling of an optical light with plasmons (or electronic excitations) on the surface of the periodically patterned metallic film. Later in Ref. 48, it was shown that by changing the nanostructured array elements, namely the refractive index of the adjacent medium and the angle of incidence, it is possible to handle optical transmission through metallic film. In this way, one can specifically design the topology of metallic structure to allow an extraordinary transmission through the spacing between ridges with a specific height of grating to thus increase the transmission of an optical excitation within a photoconductive layer. Later, Martin-Moreno et al.[49] and Shen et al.[50] carried out an analytical calculation of nanostructured configuration featuring an artificial refractive index by exploiting the subwavelength propagating modes in metallic systems. This gave rise to the possibility of calculating nanostructured configuration for the required wavelength of an optical pump excitation. Further, the theory of electromagnetic waves interaction with periodic arrays of subwavelength metallic slits has further been developed so that the grating exhibits an extraordinary electromagnetic transmission at optical and THz frequencies simultaneously.[51,52]

The aforementioned theory gave rise to an implementation of metallic metasurface featuring a 2-D grid, the so-called 2-D plasmonic grating [see Fig. 1(a)], which resulted in a strong local field enhancement in the PCA's gap.[53–55] The efficiency of this 2-D grating strongly depends on

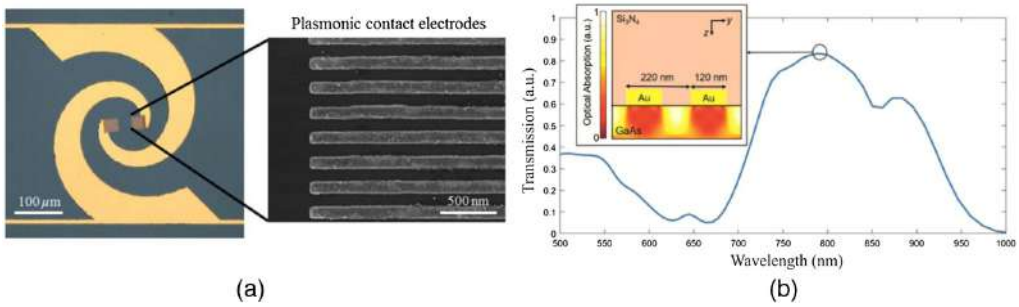

Fig. 1 (a) Optical microscopic image of the log-spiral PCA integrated with plasmonic contact electrodes and a magnified scanning electron microscopic (SEM) image of plasmonic grating (reproduced from Ref. 63, with the permission of AIP Publishing). (b) Optical transmission spectrum through the plasmonic grating. The inset denotes an optical absorption inside the photoconductive substrate at a vertical cross section at 800 nm pump wavelength [adapted from Ref. 65, with the permission of Springer Nature under a Creative Commons Attribution (CC BY) license].

the polarization of incident radiation, whereas the grating was initially designed to excite surface plasmon waves along the grating when being pumped with a TM-polarized optical wave. The latter allows the transmission of a large portion of an optical light through the nanoscale grating into a photoconductive substrate [Fig. 1(b)]. In addition, using the PCA featuring nanoscale plasmonic electrodes, one can significantly reduce the average path of photocarriers toward antenna electrodes and hence increase an optical-to-THz conversion. Later, Berry et al.[56] proposed the design of the PCA with plasmonic grating, which is widely used until now.

The grating comprised Ti/Au metallization featuring 200-nm pitch, 100-nm spacing, and 50-nm total height. The plasmonic PCA utilized a low-temperature grown (LT-GaAs) photoconductive layer with a 150-nm SiO_2 antireflection coating. The authors demonstrated a 50-fold enhancement in the emitted THz power and a 30-fold increase in the PCA-detector sensitivity compared with the conventional PCA without gratings. In addition, we note that a 2-D plasmonic grating can also be used in the PCAs in unbiased modes.[57–59]

The further improvement of the grating design was proposed in Refs. 60 and 61 by means of etching LT-GaAs in the way that high-aspect ratio gratings can be formed and their sidewalls then can be covered with metal (see Fig. 2). These so-called 3-D plasmonic electrodes featuring 400 nm height of LT-GaAs determine the excited modes inside the subwavelength slab waveguides formed by the gratings; thus higher order TEM guided modes can be excited with an optical pump excitation.[52] The authors obtained 105 μW of the emitted THz power within the 0.1- to 2.0-THz frequency bandwidth with response to 1.4 mW of an optical pump that resulted in a record-high optical-to-THz conversion of 7.5%. Nevertheless, it should be noted that 3-D plasmonic gratings require tough technological facilities and thus are difficult to fabricate.

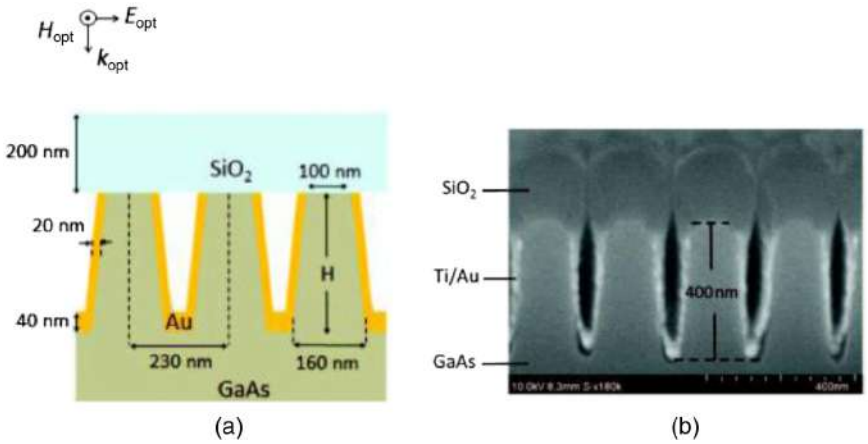

Fig. 2 (a) Schematic of the 3-D plasmonic grating and (b) its SEM image (adapted from Ref. 60, with the permission of OSA Publishing).

Alternatively to Ref. 61, Lavrukhin et al.[62] studied the PCA with optimized plasmonic grating geometry. The PCA features log-spiral Au-electrodes deposited on a SI-GaAs photoconductive substrate. The optimization was made by means of numerical simulations. The grating period was equal to 200 nm with nanoridge thickness of 100 nm, whereas plasmonic grating height was 100 nm. A 230-nm Si_3N_4 passivation under the antenna's metallization was used to reduce leakage currents through the PCA, whereas a 180-thick Al_2O_3 antireflection and protection coating layer was deposited on top of the structure. The given design of the plasmonic PCA provided a dynamic range exceeding 70 dB along with spectral bandwidth of 4 THz and a 3000-fold enhancement in the emitted THz power in the low-frequency region. We note that these spectral parameters were achieved in the operation with low optical pulses featuring an average pump power <1 mW.

The another approach is associated with the plasmonic nanoantenna arrays and can be used for generation[63,64] and detection[65] of the THz waves. The array of the plasmonic PCAs is able to significantly increase the emitted THz power by reducing thermal breakdown[66] and photocarrier screening[28] even at high energies of an optical pump. Berry et al.[63] utilized the 3×3 array of microlens, which splits and focuses the optical pump beam onto the active area of each plasmonic PCA-emitter [see Fig. 3(a)] fabricated on LT-GaAs. It was stated to reach a very high emitted THz power of up to 1.9 mW in the 0.1- to 2-THz frequency range corresponding to an optical pump power of 320 mW.

Later in Ref. 64, a large-area PCA-emitter featuring an 0.5×0.5 mm^2 active area based on a 2-D array of plasmonic nanoantennas was proposed. The emitter utilizes an ErAs:InGaAs photoconductive substrate featuring very high-resistivity and ultrashort photocarrier lifetime. The array is connected to anode bias lines within every other gap between the anode and cathode bias lines. The other gaps between the anode and cathode bias lines are shadowed by a second metal layer deposited on top of a Si_3N_4 antireflection coating layer. This blocks optical transmission into the photoconductive layer and prevents the formation of an optically induced radiating dipole moment in the opposite direction to that of the 2-D nanoantennas.[67,68] The

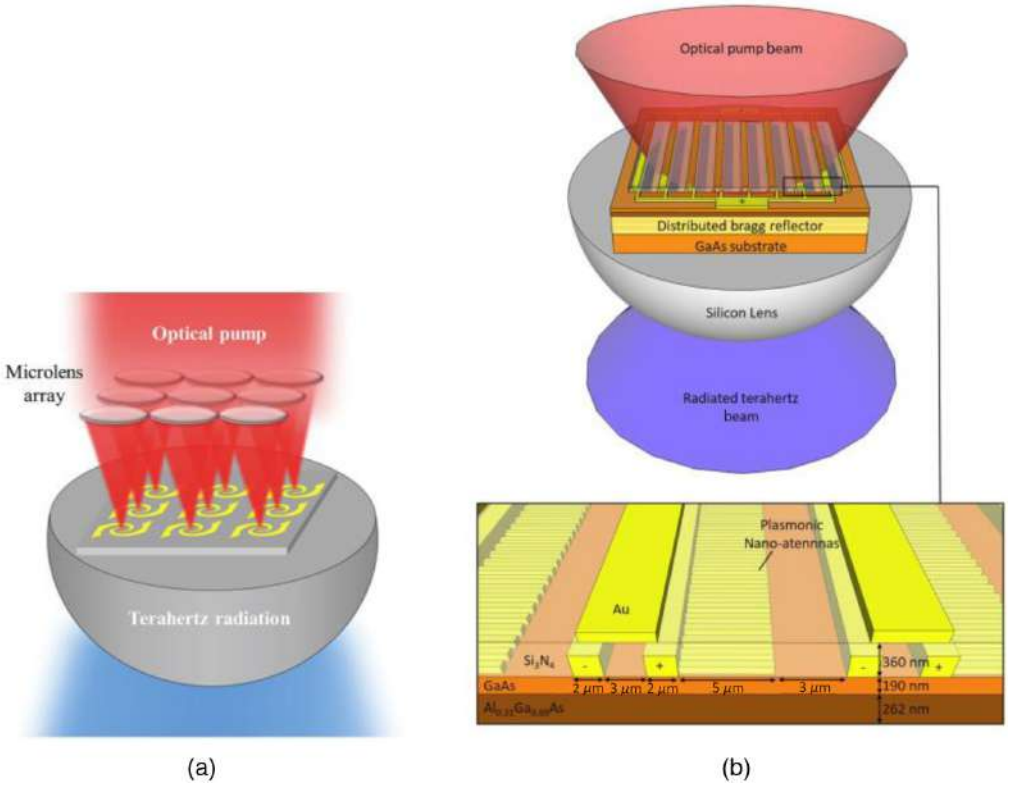

Fig. 3 (a) The 2-D array of plasmonic PCAs (reproduced from Ref. 63, with the permission of AIP Publishing). (b) The PCA featuring a 3-D plasmonic nanocavity with DBR (adapted from Ref. 1, with the permission of Springer Nature).

observed THz power exceeded 300 μW over the 0.1- to 5-THz frequency range. Yardimci and Jarrahi[65] used the similar plasmonic array topology and LT-GaAs as a photoconductive layer to extend their approach on a PCA-detector. With an implementation of a 4-μm length nanoantenna with a tip-to-tip gap size of 500 nm, one can reached a high signal-to-noise ratio (SNR) of 107 dB when operating with an optical pump power of 170 mW.

The recent progress in PCA fabrication is attributed to the plasmonic nanocavity, which induces a 3-D confinement of an optical pump pulse between a distributed Bragg reflector (DBR) at the bottom and the plasmonic nanoantenna on the top of the photoconductive layer [see Fig. 3(b), adapted from Ref. 69]. In this case, the photocarriers are generated in very close proximity to the nanoantennas, and if a bias voltage is simultaneously applied, almost all of them can reach the nanoantennas and contribute to the THz emission. Yardimci et al.[69] proposed a PCA-emitter consisting of a 2-D array of the plasmonic nanoantennas fabricated on a high-mobility 190-nm-thick GaAs photoconductive layer with a DBR. The latter comprises 25 alternating pairs of 60-nm-thick AlAs and 55-nm-thick $Al_{0.33}Ga_{0.67}As$ layers. The fabricated PCA generates 4 mW of the THz power over the 0.1- to 4-THz frequency range with respect to an optical pump power of 720 mW. Later, Yardimci et al. used this PCA configuration combined with a 170-nm thick GaAs photoconductive layer (the similar as in Ref. 69) as a PCA-detector.[70] They demonstrated an SNR of 100 dB when operating with an optical pump power of 5 mW. However, as an optical power exceeds 5 mW, the sensitivity of the detector starts saturating, whereas the LT-GaAs-based PCA-detector exhibits higher responsivities working with the same optical pump. Thus despite the great responsivity at low pump powers of up to 5 mW, the higher optical pump levels require shortening of the photocarrier lifetimes and the LT-GaAs becomes a more preferable photoconductor for the plasmonic PCA-detectors.

Recently, a very promising design of the plasmonic gratings has been theoretically proposed by Khorshidi et al.[71] They proposed modifying the plasmonic PCA with a periodic metallic grating structure by means of the three-stepped rods buried in the photoconductive layer [see Fig. 4(a)]. In accordance with the analytical results,[71] an implementation of the new grating featuring the same parameters as in Ref. 56 with the exception of the rods dimensions lead to an increase of the transmitted power of 800 nm optical excitation into the photoconductive layer from 35% to ~100% compared with the plasmonic PCA with rectangular rods. As a result, the generated THz photocurrent and the emitted THz power of the plasmonic PCA were increased up to 82% and 226%, respectively, using the buried three-stepped rods. Nevertheless, it should be noted that the practical use of the buried rods grating might be limited due to fabrication issues.

In addition, a 2-D plasmonic array with special topology can be used in an optical polarization-insensitive THz emitter. Li et al.[72] proposed an array of nanoscale cross-shaped apertures as the plasmonic contact electrodes [Fig. 4(b)]. The log-spiral antenna was deposited on a surface of the SI-GaAs photoconductive substrate. The cross-shaped plasmonic contact electrodes of antenna have a 20×20 μm^2 area covered with a 340 nm Si_3N_4 antireflection coating layer. The authors found a negligible variation in the emitted THz power, which is observed when

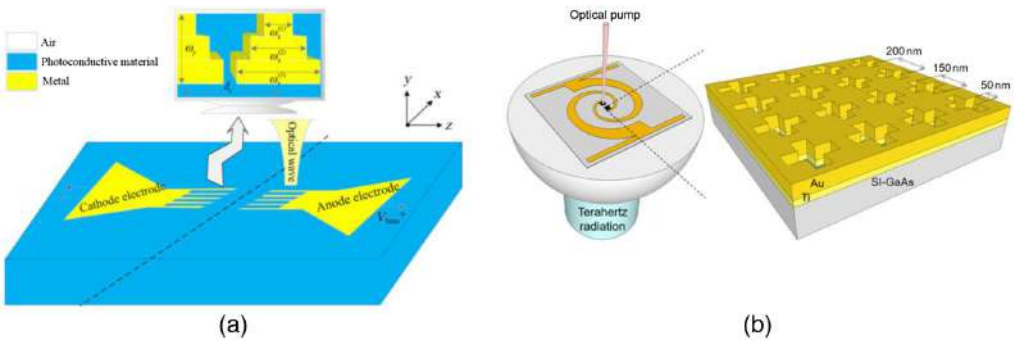

Fig. 4 (a) Schematics of the three-stepped rods buried in a photoconductive layer (adapted from Ref. 70 with the permission of OSA Publishing). (b) The array of nanoscale cross-shaped apertures with its dimensions for polarization-insensitive THz emitter [reproduced from Ref. 1, with the permission of AIP Publishing under a Creative Commons Attribution (CC BY) license].

the angle of an optical polarization varies from 0 deg to 180 deg. The emitter demonstrates the THz power of 28.4 μW at an optical pump power of 8 mW and a bias voltage of 20 V. Note that the THz power is comparable to that from Ref. 63 where the plasmonic PCA was pumped with the TM-polarized optical excitation.

It should be noted that the plasmonic effects found their application in photomixers used for CW generation and detection of the THz waves. In general, THz photomixers commonly utilize interdigitated electrodes, which allows for effectively increasing both the length of the metal–semiconductor interface and the active area for the THz generation.[73–77] Recently, using the modified photomixer electrodes featuring a tip-to-tip topology that provides strong THz field enhancement with good impedance matching to antenna and exhibits a lower RC time constant allowing the enhancement of the THz intensity in the high-frequency region of the THz spectrum was proposed.[78,79] Meanwhile, the tip-to-tip topology implies that the subwavelength electrode gaps to employ plasmonic effects to increase the electric field in close proximity to the electrodes. Seniutinasa et al.[80] proposed a photomixer in conjunction with a 800-nm laser comprising a meander-shape antenna and the sub-100-nm Au nanoelectrodes deposited on the LT-GaAs photoconductive substrate that demonstrated a few hundreds of nW at around 0.15 THz and around one order lower of nW in the 0.3- to 0.4-THz frequency range when operating with a bias voltage of 20 V and an optical pump power of 50 mW. Later in Ref. 81, a high-power photomixer in conjunction with a 1550-nm fiber laser featuring the log-spiral antenna combined with plasmonic gratings was proposed. The design of the gratings was the same as in Ref. 56 while each contact electrode had a 15×15 μm^2 area covered with a 250-nm-thick Si_3N_4 antireflection coating layer. The photomixer demonstrated up to 0.8-mW radiation power at 1 THz within every duty cycle at an optical pump power of 150 mW and a modulation frequency of 1 MHz. The same plasmonic structure was used for the heterodyne THz detector exhibiting a broadband THz detection over the 0.1- to 0.55-THz frequency range.[82]

Recently, the specifically designed interdigitated plasmonic grating was used for the THz detection.[83] The detector utilized a quasi-1-D structure featuring the undoped InGaAs photoconductive channel combined with the interdigitated nanoelectrodes that were installed every 200 nm on the mesa structure to manipulate the local ultrafast photocarrier dynamics via a carefully designed field-enhancement and plasmon effects (see Fig. 5). For comparison, the authors fabricated a reference photomixer based on 100 pairs of LT-InGaAs/InAlAs multilayers grown on a Fe-doped InP substrate. The length and the width of the fingers of the reference photomixer were equal to 8 and 1 μm, respectively, with a separation of 2.2 μm. The 10-mW optical beating signal was focused on the photoconductive regions of the photomixers. It was shown that the novel photomixer can detect CW THz radiation of up to 2 THz, which is ~10 times better than the reference photomixer.

Another promising approach implies the hybrid PCA featuring an array of metallic nanoislands or nanoantennas. To date, different kinds of hybrid PCAs have been proposed and studied both theoretically and experimentally, including rectangular[84] and hexagonal[31] nanoantennas,

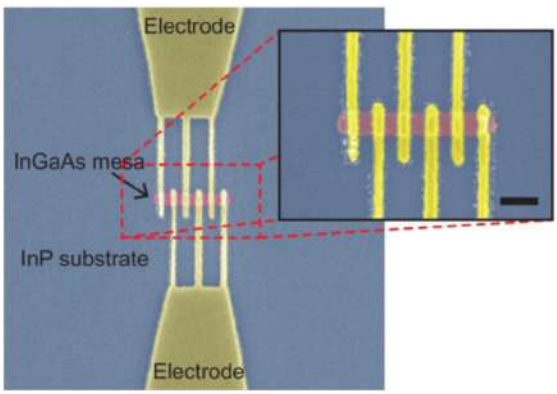

Fig. 5 SEM image of nanoplasmonic InGaAs photomixer (reproduced from Ref. 81, with the permission of AIP Publishing).

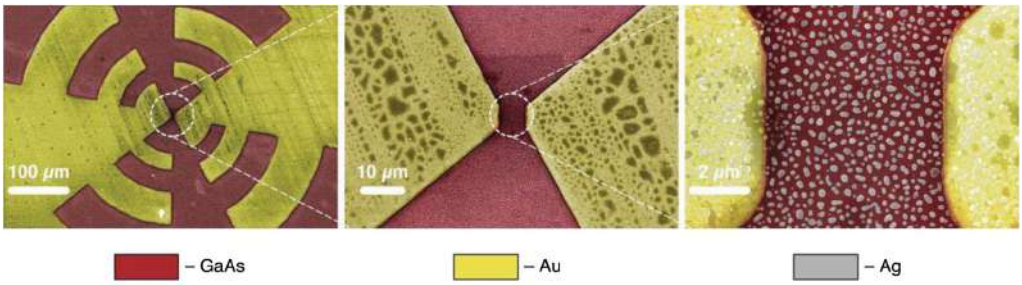

Fig. 6 SEM images of the PCA with Ag nanoislands in the photoconductive gap (adapted from Ref. 45, with the permission of Springer Nature).

Au nanodisk array,[85] and the PCAs featuring single- and double-layer topology of nanoantennas with different types and sizes.[86–88] We briefly summarize the most recent achievements.

One of the pioneer papers was dedicated to the incorporation of Ag nanoislands into the PCA gap by means of thermal dewetting of a thin metal film at relatively low temperature.[89] For a 20-nm-thick Ag film, the average diameter of Ag nanoislands amounts to ~173 nm. The fabricated PCA showed two times higher enhancement in the emitted THz power compared with the PCA without nanoislands. Later, this idea was evolved in Ref. 45, where Lepeshov et al. found the optimized size of the Ag nanoislands via numerical simulations. Typical SEM images of the PCA with Ag nanoislands are depicted in Fig. 6.

The size and the shape of the nanoislands were chosen to provide maximum absorption of an optical excitation at 800 nm. The hybrid PCAs utilized self-assembled InAs quantum dots embedded into a GaAs matrix, which are used to reduce photocarrier lifetimes.[90,91] The fabricated PCA demonstrates over a fivefold increase in the generated THz signal at around 1 THz and over a twofold increase in the overall THz power compared with the reference PCA.

A significant increase in the optical-to-THz conversion has been recently observed in the plasmonic metasurface comprising a Au nanodisks array.[92] The authors used the nanodisks height and diameter and the array's periodicity equal to 120, 230, and 420 nm, respectively; then the nanodisks were covered with Ti/Au metallization and 200 nm Si_3N_4 antireflection and passivation layer [see Fig. 7(a)]. As a result, the registered THz electric field was 5.6 times higher in the 0.1- to 2.5-THz frequency range compared with the reference PCA without the metasurface.

An interesting idea featuring the plasmonic metasurface was recently realized in Ref. 93. The H-shape THz emitter with the bowtie gap area was deposited on the top side of a 625-μm-thick photoconductive GaAs emitter. The metasurface constitutes the T-shaped resonators on the backside of the emitter. The metasurface lies below the Fraunhofer distance with respect to the excitation source and thus is excited in a quasi-near-field zone. Therefore, an extraordinary broad transmission enhancement at around 0.47 THz and another extremely narrow enhancement at 0.92 THz in the THz emission spectrum can be observed owing to the quasi-near-field excitation.

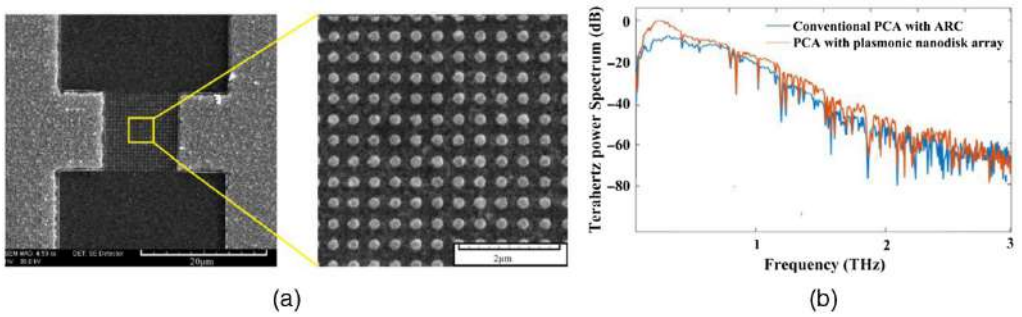

Fig. 7 (a) SEM image of the PCA with Au nanodisk array. (b) THz radiation power spectra comparison for plasmonic and conventional PCAs (adapted from Ref. 90, with permission from SPIE).

Note that the second enhancement at 0.92 THz is twice as high as that of the PCA without metasurface.

The one promising approach seems to be transparent-conducting oxides (TCOs) that can be used as a metasurface material for the PCAs due to smaller losses compared with noble metals.[94–96] Gric et al.[46] studied the absorption of a laser pulse in the PCAs with silver- and TCO-based nanocylinders inserted into GaAs volume and demonstrated that the TCO-based metasurface provides a fivefold absorption enhancement compared with the silver-based metasurface thus leading to a 25-fold increase in the emitted THz power.

3 Dielectric Metasurfaces

Alternatively to the plasmonic metasurfaces, the dielectric metasurfaces have attracted a significant interest in recent years because they can efficiently neutralize the drawbacks of plasmonic structures.

As is known, plasmonic metasurfaces suffer from low transmission efficiency due to reflections and absorption.[97] Despite dielectric structures provide lower field enhancement compared with plasmonic structures, their significant advantage is the lack of dissipation. Furthermore, the electric field hotspot can be controlled to lie either inside or outside the resonator in the near-field environment.[98] In addition, the predominantly electric dipole nature of plasmonic resonances makes it difficult to achieve any enhancement of the magnetic field.[99]

This fundamental challenge can be overcome using dielectric metasurfaces made of high-index nanoparticles. When light with frequency below or near the bandgap frequency of the material hits a high-index nanosphere, both the magnetic and electric dipole resonances are excited, making the particle behave like a magnetic dipole (first Mie resonance) and an electric dipole (second Mie resonance).[34,100] In addition, along with enhanced spectral control, dielectric metasurfaces can affect the polarization and spatial profile of beams.[101] Figure 8 illustrates schematics of the electric field distributions in plasmonic and dielectric structures.

The implementation of either dielectric particles or structures into the PCA's gap has become one of the intensively growing trends that efficiently work for both photoconductive THz emitter and detector. For instance, it has been demonstrated that silicon-based flat meta-lens directly mounted on the backside of the PCA can efficiently collimate THz waves compared with a conventional hyper-hemispherical lens due to reduced thickness and lightness offering an ease of fabrication.[102] Recently, a meta-lens featuring the dielectric metasurface with a subwavelength unit size of 0.39λ was proposed, demonstrating its competitive application in the THz imaging and focusing.[103]

In general, thin dielectric films are used in the PCAs predominantly as antireflection coating layers, reducing the Fresnel losses and thereby increasing the absorption of an optical excitation by a photoconductive substrate. The most commonly used materials have become SiO_2,[60,61] Si_3N_4,[104] and Al_2O_3. Recently, a highly electrical resistive TiO_2 was proposed as an antireflection coating in contrast to the above-mentioned materials.[105] The schematic view and an SEM

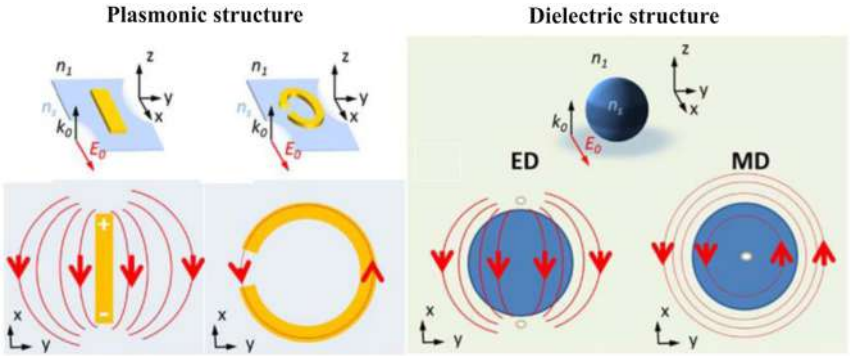

Fig. 8 Schematics of the electric field distributions in plasmonic and dielectric structures (adapted from Ref. 32 with the permission of OSA Publishing).

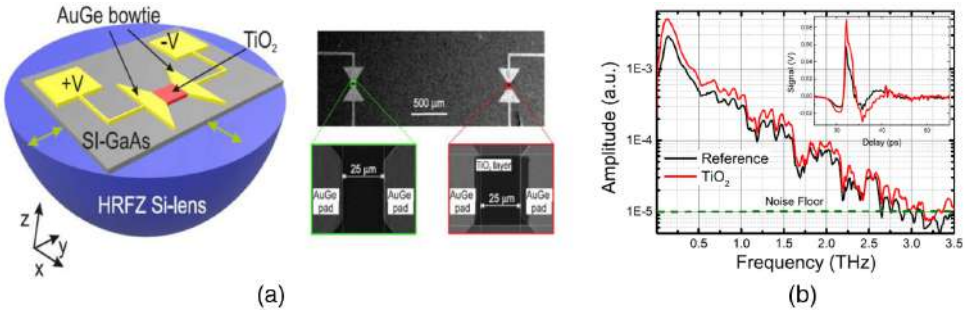

Fig. 9 (a) Schematic view of the proposed PCA with TiO_2 layer with its SEM image and (b) spectra of THz pulses emitted for TiO_2 coated and uncoated PCAs (from Ref. 103, with the permission of AIP Publishing).

image of the proposed PCA with a TiO_2 layer with its spectral characteristics are depicted in Fig. 9. The authors demonstrated that a 80-nm TiO_2 layer embedded into the PCA gap efficiently suppresses the reflection from the SI-GaAs (~6.9%), resulting in an enhancement of optical-to-THz conversion.

Further improvement of the PCA performance was proposed by Bashirpour et al.,[106] where they implemented an optical nanoantenna comprised of an array of dielectric ZnO nanorods to boost the local field and the optical absorption. This resulted in a twofold increase in the THz photocurrent and a fourfold enhancement in the emitted THz power compared with the conventional PCA without nanoantenna. Furthermore, ZnO nanorods act as a virtual layer with a spatially varying refractive index between air, an antireflection coating layer, and a photoconductive substrate to minimize the reflection. The schematic diagram of the proposed PCA and the SEM image of ZnO nanorods are depicted in Fig. 10.

In addition, it was recently stressed that the antireflection surface can be fabricated using a femtosecond laser direct writing.[107] The authors demonstrated a great suppression of a specular reflection on a sapphire with an inverted pyramid and cone arrays with a pitch of 2 μm and a total height ~900 nm.

Recently, the new-design PCA featuring a defective photonic crystal (DPC) substrate, which consists of a 2-D hexagonal lattice of air holes drilled into the thick underlying substrate, was proposed.[108] The hexagonal lattice has a defect core region, like a solid core photonic crystal waveguide, which overlaps with the excitation gap of the PCA. The authors with this proposal aimed to reduce the leaky modes (also known as substrate surface modes) and Fabry–Perot effect through a decrease in the effective dielectric constant of the substrate using the DPC. Another advantage of the DPC substrate is the enhanced directivity of the antenna because the radiation spreads mainly along the defect axis.

Rahmati and Ahmadi-Boroujeni[109] extended their proposal by designing two different PCA arrays based on the DPC substrate. Using 1×2 arrays of bow-tie and four-leaf-clover-shaped PCAs, the improvement of directivity in a broad band and the enhancement of the photomixer antenna impedance at a resonant frequency have been demonstrated.

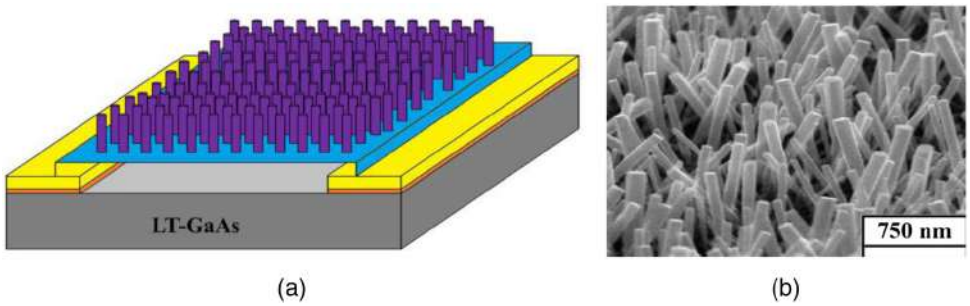

Fig. 10 (a) Schematic diagram of the proposed PCA and (b) the SEM image demonstrating ZnO nanorods (adapted from Ref. 104 with the permission of Springer Nature).

It should be emphasized that the first theoretical studies showcasing the impact of the dielectric metasurface comprised of the periodic dielectric strips embedded into the PCA's gap on the antenna performance were presented by Khorshidi and Dadashzadeh.[110] They used the developed model for the calculation of the generated THz photocurrent and the emitted THz power[111] as well as the equivalent circuit model.[112] The results demonstrate that the dielectric structure featuring strips transmits about 73% of the TE-polarized wave power, corresponding to a 800-nm fs-laser excitation, which is 7% higher compared with the power transmitted through the dielectric structure without any strips. Moreover, the power of the TM-polarized wave transmitted through the dielectric structure with the periodic strips is about 90%, which is 32% higher than the power transmitted through the dielectric structure without strips. All of these resulted in a 70% and 20% increase in the emitted THz power compared with the PCA featuring no strips. In addition, the dielectric strips allow for transferring more heat from the semiconductor to the air, thus reducing the parasitic drop off in the photocarrier lifetime and the frequency bandwidth.[113,114]

In a continuation of Ref. 110, Kazemi et al.[115] numerically demonstrated the improvement of the transmission for both TE- and TM-polarized waves by the additional incorporation of mixed graphene electrodes, which resulted in the increase of the detected THz signal. With the proposed design, the transmission through periodic dielectric slits became more than 96% and 98.65% for TE and TM polarizations, respectively. It should be noted that graphene might be attractive for the PCA[116] due to higher impedance compared with gold and copper that allows for satisfying an impedance-matching condition.[117] The latter provides an increase in both detected and emitted THz signals. It was shown that a 10-nm graphene layer placed below a 5-μm thick copper together with nanoslits allows for increasing the detected THz signal peak amplitude up to 14%.

Interestingly, that graphene can be used in the PCA-detectors to tune the THz absorbance. One of the possible solutions is the so-called graphene-uneven dielectric layered structure that provides either narrowband or broadband tunable absorption for both polarizations over a wide THz frequency band.[118] Finally, it was shown that the relative bandwidth of over 90% absorption can reach about 65% in the THz range using the nonstructured graphene loaded with geometrically gradient dielectric structures.[119]

The recent tendencies in the PCA technology aim at introduction of all-dielectric metasurfaces consisting of nanoscale Mie resonators, providing full absorption of an optical light within the selected wavelengths.[120–123]

The first PCA-detector utilizing all-dielectric metasurface was proposed by Mitrofanov et al.[124] The 20×20 μm^2 patched metasurface comprises an array of nanobeams etched on the surface of 160-nm-thick LT-GaAs featuring the period of 280 nm and the height of nanobeams

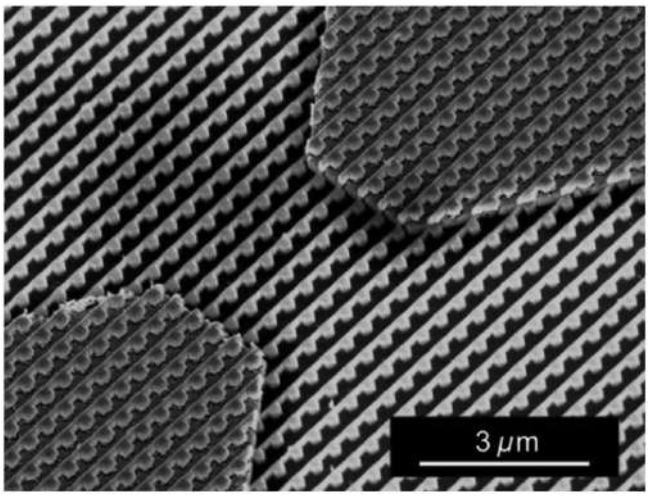

Fig. 11 SEM image illustrating the perfectly absorbing photoconductive metasurface comprising a network of resonators with broken symmetry and integrated into a THz detector [adapted with permission from Ref. 123. Copyright (2019) American Chemical Society].

equal to 70 nm. It was designed to support a confined mode and to optimize absorption of the optical excitation. The fabricated detector exhibits a 15-fold enhancement in the registered photocurrent compared with the reference one.

Recently, the aforementioned PCA-detector was further improved using a network of electrically connected GaAs resonators, which form the perfectly absorbing photoconductive metasurface.[125] The perfect absorption was achieved via cubic Mie resonators featuring the broken symmetry without any metal elements. The authors first numerically demonstrated that both odd and even magnetic dipole modes can be excited simultaneously with the metasurface compared with the rectangular (symmetric) resonator. However, the perfect absorption (98% of the incident light with a wavelength of 799 nm) is possible only for *y*-polarized light. The experimental results exhibited significant on/off switching contrast ($>10^7$), very high dark resistance ($\sim$50 GΩ), and better SNR compared with the photoconductive PCA-detector featuring no metasurface. The SEM image of the fabricated detector is shown in Fig. 11.

4 Conclusions

In this review, we briefly summarized recent and novel trends focused on metallic and dielectric metasurfaces in photoconductive THz emitters and detectors. We showcased the great potential of their application in the field of THz devices, nevertheless demonstrating limitations and technological issues. From the state-of-the-art, the metasurfaces are, by far, able to force out some previous approaches like photonic crystals and are capable of significantly increasing the performance of the contemporary photoconductive THz devices.

From comparison between metallic and dielectric metasurfaces, one can conclude that both of them demonstrate high efficiency. Nevertheless, the dielectric metasurfaces are of potential interest since they are free from dissipative ohmic losses and provide a large diversity of dielectric compounds. Moreover, the dielectric metasurface can be fabricated using a photoconductive substrate itself.[124]

In addition, we should highlight some new promising materials for the metasurfaces that are TCO. Among them are tin-doped indium oxides, gallium-doped zinc oxides, aluminum-doped zinc oxides, and others. The TCO-based plasmonic structures offer smaller ohmic losses compared with noble metals.[94–96] Nevertheless, to date, no experimental samples of the PCAs featuring plasmonic TCO-based nanoantennas have been fabricated.

It is also important to note that there are many other applications of the above-mentioned metasurfaces that lie beyond the scope of this review and that are not limited by PCAs.[126] For instance, metasurfaces can be configured for a variety of forms of light manipulation, including holograms,[127] polarization,[128] bending and focusing,[129,130] and invisible cloaks.[131,132] Concerning THz emission, different designs of the metallic metasurfaces can be used as a standalone THz emitter with no antenna metallization.[133–136] In this case, the THz generation occurs due to nonlinear optical processes[134] as well as the heat redistribution inside metal due to electron heating by an optical excitation.[137,138] However, the emitted THz power of the standalone metal metasurface is relatively low compared with the plasmonic PCA[69] and even to the surface photo-Dember THz emitter[136] and amounts, on average, to 0.15 mW, corresponding to an optical-to-THz conversion efficiency of up to 0.01% at 5.8 THz.[135] Furthermore, both metallic and dielectric metasurface configurations can be designed to effectively interact with THz radiation and thus can be used in ultrasensitive THz sensors, THz absorbers, highly selective THz detectors, tunable THz field modulators,[139–142] and THz mirrors,[143] as well as to control a wavefront at THz frequency,[144] etc.

Acknowledgments

The work on Section I by D. S. Ponomarev, A. E. Yachmenev, Yu. G. Goncharov, and D. V. Lavrukhin was supported by the Russian Science Foundation (RSF), Project No. 18-79-10195, whereas the work on Section II by R. A. Khabibullin, N. V. Zenchenko, and I. A. Glinskiy was supported by RSF, Project No. 19-79-10240. The authors are also grateful to the support of RIEC NWCRP, Grant No. H31/A31.

References

1. R. Ulbricht et al., "Carrier dynamics in semiconductors studied with time-resolved terahertz spectroscopy," *Rev. Mod. Phys.* **83**(2), 543–586 (2011).
2. P. R. Whelan et al., "Conductivity mapping of graphene on polymeric films by terahertz time-domain spectroscopy," *Opt. Express* **26**(14), 17748–17754 (2018).
3. G. A. Komandin et al., "Electrodynamical characteristics of α-lactose monohydrate in the terahertz range," *Opt. Spectrosc.* **126**(5), 514–522 (2019).
4. A. M. Kuzmenko et al., "Terahertz spectroscopy of crystal-field transitions in magnetoelectric $TmAl_3(BO_3)_4$," *Phys. Rev. B Condens. Matter* **94**(17), 174419 (2016).
5. C. D. Stoik et al., "Nondestructive evaluation of aircraft composites using transmissive terahertz time domain spectroscopy," *Opt. Express* **16**(21), 17039–17051 (2008).
6. E. V. Yakovlev et al., "Non-destructive evaluation of polymer composite materials at the manufacturing stage using terahertz pulsed spectroscopy," *IEEE Trans. Terahertz Sci. Technol.* **5**(5), 810–816 (2015).
7. V. L. Vaks et al., "Exhaled breath analysis: physical methods, instruments, and medical diagnostics," *Phys. Usp.* **57**(7), 684–701 (2014).
8. A. A. Yablokov et al., "Two-frequency THz spectroscopy for analytical and dynamical research," *IEEE Trans. Terahertz Sci. Technol.* **5**(5), 845–851 (2015).
9. E. Sobakinskaya et al., "High-resolution terahertz spectroscopy with a noise radiation source based on high-T superconductors," *J. Phys. D Appl. Phys.* **50**(3), 035305 (2017).
10. J. A. Zeitler et al., "Terahertz pulsed spectroscopy and imaging in the pharmaceutical setting—a review," *J. Pharm. Pharmacol.* **59**(2), 209–223 (2007).
11. K. Kawase et al., "Non-destructive terahertz imaging of illicit drugs using spectral fingerprints," *Opt. Express* **11**(20), 2549–2554 (2003).
12. K. Ahi et al., "Quality control and authentication of packaged integrated circuits using enhanced-spatial-resolution terahertz time-domain spectroscopy and imaging," *Opt. Lasers Eng.* **104**, 274–284 (2018).
13. I. N. Dolganova et al., "A hybrid continuous-wave terahertz imaging system," *Rev. Sci. Instrum.* **86**(11), 113704 (2015).
14. I. N. Dolganova et al., "The role of scattering in quasi-ordered structures for terahertz imaging: local order can increase an image quality," *IEEE Trans. Terahertz Sci. Technol.* **8**(4), 403–409 (2018).
15. I. V. Minin and O. V. Minin "System of microwave radiovision of three-dimensional objects in real time," *Proc. SPIE* **4129**, 616–619 (2000).
16. I. V. Minin and O. V. Minin, "THz quasi-optics applications in security," *Proc. SPIE* **6212**, 621210 (2006).
17. X. Yang et al., "Biomedical applications of terahertz spectroscopy and imaging," *Trends Biotechnol.* **34**(10), 810–824 (2016).
18. K. I. Zaytsev et al., "In vivo terahertz spectroscopy of pigmentary skin nevi: pilot study of non-invasive early diagnosis of dysplasia," *Appl. Phys. Lett.* **106**(5), 053702 (2015).
19. O. A. Smolyanskaya et al., "Terahertz biophotonics as a tool for studies of dielectric and spectral properties of biological tissues and liquids," *Prog. Quantum Electron.* **62**, 1–77 (2018).
20. A. A. Gavdush et al., "Terahertz spectroscopy of gelatin-embedded human brain gliomas of different grades: a road toward intraoperative THz diagnosis," *J. Biomed. Opt.* **24**(2), 027001 (2019).
21. N. V. Chernomyrdin et al., "Reflection-mode continuous-wave 0.15λ-resolution terahertz solid immersion microscopy of soft biological tissues," *Appl. Phys. Lett.* **113**(11), 111102 (2018).
22. K. I. Zaytsev et al., "The progress and perspectives of terahertz technology for diagnosis of neoplasms: a review," *J. Opt.* in press (2019).
23. H. Guerboukha et al., "Toward real-time terahertz imaging," *Adv. Opt. Photonics* **10**(4), 843–938 (2018).
24. O. V. Minin and I. V. Minin, "Ultrafast all-optical THz modulation based on wavelength scaled dielectric particle with graphene monolayer," *Proc. SPIE* **11065**, 110651J (2019).

25. J. Pozhela and A. Reklaitis, "Electron transport properties in GaAs at high electric fields," *Solid State Electron.* **23**, 927–933 (1980).
26. M. Beard et al., "Subpicosecond carrier dynamics in low-temperature grown GaAs as measured by time-resolved terahertz spectroscopy," *J. Appl. Phys.* **90**, 5915–5923 (2001).
27. D. S. Ponomarev et al., "Enhanced terahertz emission from strain-induced InGaAs/InAlAs superlattices," *J. Appl. Phys.* **125**(15), 151605 (2019).
28. G. C. Loata et al., "Radiation field screening in photoconductive antennae studied via pulsed terahertz emission spectroscopy," *Appl. Phys. Lett.* **91**(23), 232506 (2007).
29. N. M. Burford and M. O. El-Shenawee, "Review of terahertz photoconductive antenna technology," *Opt. Eng.* **56**(1), 010901 (2017).
30. T. Hattori et al., "Intense terahertz pulses from large-aperture antenna with interdigitated electrodes," *Jpn. J. Appl. Phys.* **45**, L422–L424 (2006).
31. A. Jooshesh et al., "Nanoplasmonics enhanced terahertz sources," *Opt. Express* **22**(23), 27992–28001 (2014).
32. P. Genevet et al., "Recent advances in planar optics: from plasmonic to dielectric metasurfaces," *Optica* **4**(1), 139–152 (2017).
33. S. Jahani and Z. Jacob, "All-dielectric metamaterials," *Nat. Nanotechnol.* **11**, 23–36 (2016).
34. I. V. Minin and O. V. Minin, *Diffractive Optics and Nanophotonics: Resolution below the Diffraction Limit*, Springer, Cham (2016).
35. I. V. Minin et al., "Photonic hook plasmons: a new curved surface wave," *Ann. Phys.* **530**(12), 1800359 (2018).
36. L. Cong et al., "All-optical active THz metasurfaces for ultrafast polarization switching and dynamic beam splitting," *Light Sci. Appl.* **7**, 28 (2018).
37. I. V. Minin et al., "Experimental observation of a photonic hook," *Appl. Phys. Lett.* **114**(3), 031105 (2019).
38. Y. Cao et al., "Deep subwavelength-scale light focusing and confinement in nanohole-structured mesoscale dielectric spheres," *Nanomaterials* **9**(2), 186 (2019).
39. A. Pors et al., "Broadband focusing flat mirrors based on plasmonic gradient metasurfaces," *Nano Lett.* **13**, 829–834 (2013).
40. D. Fattal et al., "Flat dielectric grating reflectors with focusing abilities," *Nat. Photonics* **4**, 466–470 (2010).
41. A. Arbabi et al., "Dielectric metasurfaces for complete control of phase and polarization with subwavelength spatial resolution and high transmission," *Nat. Nanotechnol.* **10**, 937–943 (2015).
42. M. I. Shalaev et al., "High-efficiency all-dielectric metasurfaces for ultracompact beam manipulation in transmission mode," *Nano Lett.* **15**, 6261–6266 (2015).
43. M. Kerker et al., "Electromagnetic scattering by magnetic spheres," *J. Opt. Soc. Am.* **73**(6), 765–767 (1983).
44. T. Gric, "Surface-plasmon-polaritons at the interface of nanostructured metamaterials," *Prog. Electromagn. Res. M* **46**, 165–172 (2016).
45. S. Lepeshov et al., "Boosting terahertz photoconductive antenna performance with optimised plasmonic nanostructures," *Sci. Rep.* **8**, 6624 (2018).
46. T. Gric et al., "Tunable plasmonic properties and absorption enhancement in terahertz photoconductive antenna based on optimized plasmonic nanostructures," *Int. J. Infrared Millimeter Waves* **39**, 1028–1038 (2018).
47. T. W. Ebbesen et al., "Extraordinary optical transmission through sub-wavelength hole arrays," *Nature* **391**, 667–669 (1998).
48. T. Kim et al., "Control of optical transmission through metals perforated with subwavelength hole arrays," *Opt. Lett.* **24**, 256–258 (1999).
49. L. Martin-Moreno et al., "Theory of extraordinary optical transmission through subwavelength hole arrays," *Phys. Rev. Lett.* **86**, 1114–1117 (2001).
50. J. T. Shen et al., "Mechanism for designing metallic metamaterials with a high index of refraction," *Phys. Rev. Lett.* **94**, 197401 (2005).
51. C. W. Berry et al., "Design of reconfigurable metallic slits for terahertz beam modulation," *Opt. Express* **19**, 1236–1245 (2011).

52. B.-Y. Hsieh and M. Jarrahi, "Analysis of periodic metallic nano-slits for efficient interaction of terahertz and optical waves at nano-scale dimensions," *J. Appl. Phys.* **109**, 084326 (2011).
53. C. W. Berry and M. Jarrahi, "Plasmonically-enhanced localization of light into photoconductive antennas," in *CLEO/QELS: Laser Sci. Photonic Appl.*, pp. 1–2 (2010).
54. C. W. Berry and M. Jarrahi, "Terahertz generation using plasmonic photoconductive gratings," *New J. Phys.* **14**, 105029 (2012).
55. B. Heshmat et al., "Nanoplasmonic terahertz photoconductive switch on GaAs," *Nano Lett.* **12**(12), 6255–6259 (2012).
56. C. W. Berry et al., "Significant performance enhancement in photoconductive terahertz optoelectronics by incorporating plasmonic contact electrodes," *Nat. Commun.* **4**, 1622 (2013).
57. A. Jooshesh et al., "Plasmon-enhanced LT-GaAs/AlAs heterostructure photoconductive antennas for sub-bandgap terahertz generation," *Opt. Express* **25**, 22140–22148 (2017).
58. F. Fesharaki et al., "Plasmonic antireflection coating for photoconductive terahertz generation," *ACS Photonics* **4**(6), 1350–1354 (2017).
59. B. Heshmat et al., "Enhanced terahertz bandwidth and power from GaAsBi-based sources," *Adv. Opt. Mater.* **1**(10), 714–719 (2013).
60. S.-H. Yang and M. Jarrahi, "Enhanced light-matter interaction at nanoscale by utilizing high-aspect-ratio metallic gratings," *Opt. Lett.* **38**, 3677–3679 (2013).
61. S.-H. Yang et al., "7.5% optical-to-terahertz conversion efficiency offered by photoconductive emitters with three-dimensional plasmonic contact electrodes," *IEEE Trans. Terahertz Sci. Technol.* **4**(5), 575–581 (2014).
62. D. V. Lavrukhin et al., "Terahertz photoconductive emitter with dielectric-embedded high-aspect-ratio plasmonic grating for operation with low-power optical pumps," *AIP Adv.* **9**, 015112 (2019).
63. C. W. Berry et al., "Generation of high power pulsed terahertz radiation using a plasmonic photoconductive emitter array with logarithmic spiral antennas," *Appl. Phys. Lett.* **104**, 081122 (2014).
64. N. Yardimci et al., "High power telecommunication-compatible photoconductive terahertz emitters based on plasmonic nano-antenna arrays," *Appl. Phys. Lett.* **109**, 191103 (2016).
65. N. T. Yardimci and M. Jarrahi, "High sensitivity terahertz detection through large-area plasmonic nano-antenna arrays," *Sci. Rep.* **7**, 42667 (2017).
66. A. W. Jackson et al., "Reduced thermal conductivity in low-temperature-grown GaAs," *Appl. Phys. Lett.* **74**, 2325–2327 (1999).
67. A. Dreyhaupt et al., "High-intensity terahertz radiation from a microstructured large-area photoconductor," *Appl. Phys. Lett.* **86**, 121114 (2005).
68. M. Beck et al., "Impulsive terahertz radiation with high electric fields from an amplifier-driven large-area photoconductive antenna," *Opt. Express* **18**, 9251–9257 (2010).
69. N. T. Yardimci et al., "A high power broadband terahertz source enabled by three-dimensional light confinement in a plasmonic nanocavity," *Sci. Rep.* **7**, 4166 (2017).
70. N. T. Yardimci et al., "A high-responsivity and broadband photoconductive terahertz detector based on a plasmonic nanocavity" *Appl. Phys. Lett.* **113**, 251102 (2018).
71. M. Khorshidi et al., "Increase in terahertz radiation power of plasmonic photoconductive antennas by embedding buried three-stepped rods in electrodes," *Opt. Express* **27**, 22327–22338 (2019).
72. X. Li et al., "A polarization-insensitive plasmonic photoconductive terahertz emitter," *AIP Adv.* **7**, 115113 (2017).
73. E. A. Michael et al., "Large-area traveling-wave photonic mixers for increased continuous terahertz power," *Appl. Phys. Lett.* **86**, 111120 (2005).
74. Y. Hou et al., "Terahertz generation using implanted InGaAs photomixers and multi-wavelength quantum dot lasers," *Nano-Micro Lett.* **4**(1), 10–13 (2012).
75. K. A. McIntosh et al., "Terahertz photomixing with diode lasers in low-temperature-grown GaAs," *Appl. Phys. Lett.* **67**(26), 3844–3846 (1995).
76. I. S. Gregory et al., "Optimization of photomixers and antennas for continuous-wave terahertz emission," *IEEE J. Quantum Electron.* **41**(5), 717–728 (2005).

77. A. F. Olvera et al., "International system of units (SI) traceable noise-equivalent power and responsivity characterization of continuous wave ErAs:InGaAs photoconductive terahertz detectors," *Photonics* **6**(1), 15 (2019).
78. H. Tanoto et al., "Nano-antenna in a photoconductive photomixer for highly efficient continuous wave terahertz emission," *Sci. Rep.* **3**, 2824 (2013).
79. N. Khiabani et al., "A novel sub-THz photomixer with nano-trapezoidal electrodes," *IEEE Trans. Terahertz Sci. Technol.* **4**(4), 501–508 (2014).
80. G. Seniutinasa et al., "THz photomixer with a 40-nm-wide nanoelectrode gap on low-temperature grown GaAs," *Proc. SPIE* **8923**, 892322 (2013).
81. C. W. Berry et al., "High power terahertz generation using 1550 nm plasmonic photomixers," *Appl. Phys. Lett.* **105**, 011121 (2014).
82. N. Wang and M. Jarrahi, "Broadband heterodyne terahertz detector based on plasmonic photomixing," in *41st Int. Conf. Infrared, Millimeter, and Terahertz Waves* (2016).
83. K. Moon et al., "Photo-conductive detection of continuous THz waves via manipulated ultrafast process in nanostructures," *Appl. Phys. Lett.* **112**, 031102 (2018).
84. H. Surdi et al., "Enhancement of terahertz emission using auge nano-patterns," in *Proc. COMSOL Conf.*, Bangalore (2013).
85. N. M. Burford et al., "Plasmonic nanodisk thin-film terahertz photoconductive antenna," *IEEE Trans. Terahertz Sci. Technol.* **8**, 237–247 (2018).
86. S. Ghorbani et al., "Simulation of THz photoconductive antennas loaded by different metallic nano-particles," in *Fourth Int. Conf. Millimeter-Wave Terahertz Technol.*, pp. 62–64 (2016).
87. M. Bashirpour et al., "Enhancement of optical absorption in LT-GaAs by double layer nanoplasmonic array in photoconductive antenna," *Vacuum* **146**, 430–436 (2017).
88. S. Ghorbani et al., "Thin film tandem nanoplasmonic photoconductive antenna for high performance terahertz detection," *Superlattices Microstruct.* **120**, 598–604 (2018).
89. S. G. Park et al., "Terahertz photoconductive antenna with metal nanoislands," *Opt. Express* **20**(23), 25530–25535 (2012).
90. R. R. Leyman et al., "Quantum dot materials for terahertz generation applications," *Laser Photonics Rev.* **10**, 772–779 (2016).
91. K. A. Fedorova et al., "Compact all-quantum-dot-based tunable THz laser source," *IEEE J. Sel. Top. Quantum Electron.* **23**, 1–5 (2017).
92. M. Bashirpour et al., "Terahertz radiation enhancement in dipole photoconductive antenna on LT-GaAs using a gold plasmonic nanodisk array," *Opt. Laser Technol.* **120**, 105726 (2019).
93. Z. Zhao et al., "Terahertz selective emission enhancement from a metasurface-coupled photoconductive emitter in quasi-near-field zone," *Plasmonics* 1–7 (2019).
94. G. V. Naik et al., "Oxides and nitrides as alternative plasmonic materials in the optical range," *Opt. Mater. Express* **1**, 1090–1099 (2011).
95. S. Franzen, "Surface plasmon polaritons and screened plasma absorption in indium tin oxide compared to silver and gold," *J. Phys. Chem. C* **112**, 6027–6032 (2008).
96. J. Kim et al., "Plasmonic resonances in nanostructured transparent conducting oxide films," *IEEE J. Sel. Top. Quantum Electron.* **19**(3), 13474514 (2013).
97. F. Aieta et al., "Aberration-free ultrathin flat lenses and axicons at telecom wavelengths based on plasmonic metasurfaces," *Nano Lett.* **12**, 4932–4936 (2012).
98. Y. Yang et al., "All-dielectric metasurface analogue of electromagnetically induced transparency," *Nat. Commun.* **5**, 5753 (2014).
99. N. Yu and F. Capasso, "Flat optics with designer metasurfaces," *Nat. Mater.* **13**, 139–150 (2014).
100. A. Krasnok et al., "All-dielectric optical nanoantennas," *Opt. Express* **20**(18), 20599–20604 (2012).
101. S. Jahani and Z. Jacob, "Transparent subdiffraction optics: nanoscale light confinement without metal," *Optica* **1**, 96–100 (2014).
102. Q. Yu et al., "All-dielectric meta-lens designed for photoconductive terahertz antennas," *IEEE Photonics J.* **9**(4), 1–9 (2017).

103. X. Jiang et al., "All-dielectric metalens for terahertz wave imaging," *Opt. Express* **26**(11), 14132–14142 (2018).
104. C. Headley et al., "Improved performance of GaAs-based terahertz emitters via surface passivation and silicon nitride encapsulation," *IEEE J. Sel. Top. Quantum Electron.* **17**, 17–21 (2011).
105. A. Gupta et al., "Enhanced optical-to-THz conversion efficiency of photoconductive antenna using dielectric nano-layer encapsulation," *APL Photonics* **3**, 051706 (2018).
106. M. Bashirpour et al., "Photoconductive antenna using optical antenna array of ZnO nanorods," *Sci. Rep.* **9**, 1414 (2019).
107. Q.-K. Li et al., "Fabrication of an anti-reflective microstructure on sapphire by femtosecond laser direct writing," *Opt. Lett.* **42**(3), 543–546 (2017).
108. E. Rahmati and M. Ahmadi-Boroujeni, "Improving the efficiency and directivity of THz photoconductive antennas by using a defective photonic crystal substrate," *Opt. Commun.* **412**, 74–79 (2018).
109. E. Rahmati and M. Ahmadi-Boroujeni, "Design of terahertz photoconductive antenna arrays based on defective photonic crystal substrates," *Opt. Laser Technol.* **114**, 89–94 (2019).
110. M. Khorshidi and G. Dadashzadeh, "Dielectric structure with periodic strips for increasing radiation power of photoconductive antennas: theoretical analysis," *J. Infrared Millimeter Terahertz Waves* **38**, 609–629 (2017).
111. M. Khorshidi and G. Dadashzadeh, "Plasmonic photoconductive antennas with rectangular and stepped rods: a theoretical analysis," *J. Opt. Soc. Am. B* **33**(12), 2502–2511 (2016).
112. N. Khiabani et al., "Theoretical modeling of a photoconductive antenna in a terahertz pulsed system," *IEEE Trans. Antennas Propag.* **61**(4), 1538–1546 (2013).
113. E. Michael and M. Mikulics, "Losses from long-living photoelectrons in terahertz-generating continuous-wave photomixers," *Appl. Phys. Lett.* **100**(19), 191112 (2012).
114. M. Mikulics et al., "Ultrafast low-temperature-grown epitaxial GaAs photodetectors transferred on flexible plastic substrates," *IEEE Photonics Technol. Lett.* **17**(8), 1725–1727 (2005).
115. A. H. Kazemi et al., "Peak amplitude enhancement of photoconductive antenna using periodic nanoslit and graphene in the THz band," *Optik* **185**, 114–120 (2019).
116. F. Zangeneh-Nejad and R. Safian, "Significant enhancement in the efficiency of photoconductive antennas using a hybrid graphene molybdenum disulphide structure," *J. Nanophotonics* **10**(3), 036005 (2016).
117. D. Lavrukhin et al., "Shaping the spectrum of terahertz photoconductive antenna by frequency-dependent impedance matching," *Semicond. Sci. Technol.* **34**(3), 034005 (2019)
118. B.-Z. Xu et al., "A novel structure for tunable terahertz absorber based on graphene," *Opt. Express* **21**(20), 23803–23811 (2013).
119. J. Yang et al., "Broadband terahertz absorber based on multi-band continuous plasmon resonances in geometrically gradient dielectric-loaded graphene plasmon structure," *Sci. Rep.* **8**, 3239 (2018).
120. D. G. Baranov et al., "Coherent perfect absorbers: linear control of light with light," *Nat. Rev. Mater.* **2**(12), 17064 (2017).
121. M. A. Cole et al., "Terahertz absorption in all-dielectric Huygens' metasurfaces," *Nanotechnology* **27**(42), 424003 (2016).
122. X. Ming et al., "Degenerate critical coupling in all-dielectric metasurface absorbers," *Opt. Express* **25**(20), 24658–24669 (2017).
123. Y. Geints et al., "Apodization-assisted subdiffraction near-field focusing in 2D phase diffraction grating," *Ann. Phys.* **531**(7), 1900033 (2019).
124. O. Mitrofanov et al., "Efficient photoconductive terahertz detector with all-dielectric optical metasurface," *APL Photonics* **3**, 051703 (2018).
125. T. Siday et al., "Terahertz detection with perfectly-absorbing photoconductive metasurface," *Nano Lett.* **19**(5), 2888–2896 (2019).
126. L. Wang et al., "A review of THz modulators with dynamic tunable metasurfaces," *Nanomaterials* **9**, 965 (2019).
127. X. Ni et al., "Metasurface holograms for visible light," *Nat. Commun.* **4**, 2807 (2013).

128. J. P. Balthasar Mueller et al., "Metasurface polarization optics: independent phase control of arbitrary orthogonal states of polarization," *Phys. Rev. Lett.* **118**(11), 113901 (2017).
129. X. Yin et al., "Photonic spin Hall effect at metasurfaces," *Science* **339**(6126), 1405–1407 (2013).
130. A. Shaltout et al., "Photonic spin Hall effect in gap-plasmon metasurfaces for on-chip chiroptical spectroscopy," *Optica* **2**(10), 860 (2015).
131. X. Ni et al., "An ultrathin invisibility skin cloak for visible light," *Science* **349**(6254), 1310–1314 (2015).
132. L. Y. Hsu et al., "Extremely thin dielectric metasurface for carpet cloaking," *Prog. Electromagn. Res.* **152**, 33–40 (2015).
133. Y. Gao et al., "Analysis of terahertz generation via nanostructure enhanced plasmonic excitations," *J. Appl. Phys.* **106**, 074302 (2009).
134. G. K. P. Ramanandan et al., "Emission of terahertz pulses from nanostructured metal surfaces," *J. Phys. D Appl. Phys.* **47**, 374003 (2014).
135. M. Tymchenko et al., "Highly-efficient THz generation using nonlinear plasmonic metasurfaces," *J. Opt.* **19**, 104001 (2017).
136. K. Takano et al., "Terahertz emission from gold nanorods irradiated by ultrashort laser pulses of different wavelengths," *Sci. Rep.* **9**, 3280 (2019).
137. D. A. Fadeev et al., "Terahertz emission from metal nanoparticle array," *Opt. Lett.* **43**, 1939–1942 (2018).
138. I. V. Oladyshkin et al., "Optical excitation of surface plasmons and terahertz emission from metals," *Phys. Rev. B* **100**, 085421 (2019).
139. J. He and Y. Zhang, "Metasurfaces in terahertz waveband," *J. Phys. D Appl. Phys.* **50**, 464004 (2017).
140. J. Kang et al., "Terahertz wave interaction with metallic nanostructures," *Nanophotonics* **7**(5), 763–793 (2018).
141. R. Xu et al., "Tunable ultra-narrowband terahertz perfect absorber by using metal-insulator-metal microstructures," *Results Phys.* **13**, 102176 (2019).
142. X. Li et al., "Switchable multifunctional terahertz metasurfaces employing vanadium dioxide," *Sci. Rep.* **9**, 5454 (2019).
143. Z. Ma et al., "Terahertz all-dielectric magnetic mirror metasurfaces," *ACS Photonics* **3**(6), 1010–1018 (2016).
144. R. Dharmavarapu et al., "All-dielectric metasurface for wavefront control at terahertz frequencies," *Proc. SPIE* **10456**, 104561W (2018).

Alexander E. Yachmenev received his PhD from the Institute of Physics and Technology of the Russian Academy of Sciences, Moscow, Russia. He is currently a senior researcher at the V.G. Mokerov Institute of Ultra High Frequency Semiconductor Electronics of RAS (IUHFSE RAS), Moscow, Russia. His research interests include semiconductor fabrication and device modeling.

Denis V. Lavrukhin works as a researcher at IUHFSE RAS. He specializes in photoconductive THz device fabrication and pulse time-domain spectroscopy.

Igor A. Glinskiy is currently a PhD student at IUHFSE RAS. His research interests include THz technology and problems of electromagnetic wave scattering.

Nikolay V. Zenchenko is currently a PhD student at IUHFSE RAS. He works on computational modeling of different physical phenomena in various semiconductors.

Yurii G. Goncharov received his PhD from the Prokhorov General Physics Institute, Russian Academy of Sciences (GPI RAS), Moscow, Russia, where he is currently a senior researcher. His research activities focus on the development of methods and techniques for measuring the electrodynamic response of materials at millimeter–submillimeter wavelengths.

Igor E. Spektor received his PhD from the Moscow Technical Institute of Forestry, Korolev, Moscow, Russia. Since 1998, he has been at the GPI RAS, where he is the head of the laboratory. His research interests include methods and devices for BWO spectroscopy.

Rustam A. Khabibullin received his PhD from MIREA-Russian Technological University (MIREA-RTU), Moscow, Russia. He is currently a leading researcher at IUHFSE RAS and at Bauman Moscow State Technical University, Moscow, Russia. His research interests include THz technology and THz quantum-cascade lasers.

Taiichi Otsuji received his PhD from the Tokyo Institute of Technology, Tokyo, Japan. In 1999, he joined the Kyushu Institute of Technology, as an associate professor, where he became a professor in 2002. Since 2005, he has been a professor at the Research Institute of Electrical Communication, Tohoku University, Sendai, Japan. He has authored and co-authored more than 400 research publications. His current research interests include THz electronic and photonic materials/devices and their applications.

Dmitry S. Ponomarev received his PhD from MIREA-RTU. He is currently a deputy director for science at IUHFSE RAS and a leading researcher at GPI RAS and at the Moscow Institute of Physics and Technology, Dolgoprudny, Russia. His research interests include photoconductive THz emitters and detectors and THz spectroscopy and imaging.